Hypersensitivity of Southern Ocean air-sea carbon fluxes to turbulent diapycnal mixing

Elizabeth Ellison, Ali Mashayek, Matthew Mazloff

[1]Imperial College London, Department of Civil and Environmental Engineering, London, SW7 2BX, Uk
[2]Imperial College London, Department of Civil and Environmental Engineering, London, SW7 2BX, Uk
[3]Scripps Institute of Oceanography

Key Points:

- Air-sea carbon fluxes in the Southern Ocean are hypersensitive to modest background mixing variations on annual time scales
- Further carbon flux observations are required to better constrain diapycnal mixing rates
- It is essential climate models are able to resolve the spatiotemporal variability of small scale turbulent mixing in the Southern Ocean or skillfully parameterize them to model SO air sea carbon fluxes.

Corresponding author: E.Ellison, ece1818@ic.ac.uk

Abstract

The Southern Ocean (SO) connects major ocean basins and hosts large air-sea carbon fluxes due to the resurfacing of deep nutrient and carbon rich waters, driven by strong surface winds. Vertical mixing in the SO, induced by breaking waves excited by strong surface winds and interaction of tides, jets and eddies with rough topography, has been considered of secondary importance for the global meridional overturning circulation. Its importance for biological cycles has largely been assumed to be due to the role of mixing in changing the underlying dynamics on a centennial timescale. Using an eddy-resolving ocean model that assimilates an extensive array of observations, we show that altered mixing can cause up to a 40% change in SO air-sea fluxes in only a few years through altering the distribution of dissolved inorganic carbon, alkalinity, temperature and salinity. Such enhanced mixing may be induced by the propagation of tidal waves from around the globe to the SO as well as the flux of wave energy from the deep SO to shallow depths. Such processes are unresolved in climate models, yet essential.

Introduction

The Southern Ocean (SO) is a key region for the global carbon cycle due to the upwelling of deep old carbon and nutrient enriched waters, connecting the vast reservoir of nutrients and carbon from below the mixed layer with the surface(Marshall & Speer, 2012; Talley et al., 2016). The deep ocean interacts with the atmosphere through less than 4% of the oceans surface area (Watson & Naveira Garabato, 2006; Klocker, 2018), with 65% of interior waters making first contact with the atmosphere in the SO(DeVries & Primeau, 2011). As the deep ocean contains up to 60 times more carbon than the atmosphere (Intergovernmental Panel on Climate Change, 2014), very small perturbations to air sea fluxes can be important for atmospheric carbon content (Adkins, 2013). The SO is also believed to absorb 40% of the total ocean uptake of anthropogenic carbon dioxide (CO_2) each year(Devries, 2014). Therefore the SO, and especially the upwelling branch of circumpolar deep water(Marshall & Speer, 2012), is key in controlling global biogeochemical cycles, the exchange of CO_2 between the atmosphere and the deep ocean, atmospheric CO_2 levels, and the response of the ocean and atmosphere to climate change (Sarmiento et al., 2004; Gruber et al., 2019).

Cross-density (diapycnal) mixing due to breaking of oceanic internal waves is believed to be an important contributor to variations in atmospheric carbon levels on millennial timescales (Sigman et al., 2010; Marinov & Gnanadesikan, 2011). While mixing in the SO is believed to be of secondary (yet significant) importance for the Meridional Overturning Circulation (MOC) volume transport (Nikurashin & Vallis, 2011; Cessi, 2019), it has been suggested to be of leading order importance for tracer budgets(Garabato et al., 2007; Cimoli et al., 2021). The distribution of conservative and non-conservative tracers in models have been shown to be sensitive to ocean circulation and ventilation (Doney et al., 2004; Gnanadesikan et al., 2004; Talley et al., 2016). Enhanced mixing increases the deep ocean ventilation via the SO and reduces ocean carbon storage through the biological and solubility carbon pumps (Marinov et al., 2008; Marinov & Gnanadesikan, 2011). These reported changes to atmospheric CO_2 levels are all due to the role of interior mixing in altering the oceanic circulation over centennial to millennial timescales. Climate models are highly sensitive to the intensity and distribution of diapycnal mixing, accounting for about 25% of the uncertainty in the estimated range of atmospheric CO_2 concentrations by 2100(Schmittner et al., 2009).

Despite several SO expeditions having revealed strong diapycnal mixing in the SO (Garabato et al., 2004; Ledwell et al., 2011; Watson et al., 2013; Garabato et al., 2019), measurements remain sparse and difficult to scale up (Tamsitt et al., 2018). Our best estimates of mixing that cover the whole SO are based on 'static' maps produced on theoretical grounds and with many limiting assumptions (Nikurashin & Ferrari, 2010; Al-

ford, 2003; Shakespeare, 2020). While such maps have formed the base of our representation of such processes in earth system models (Melet et al., 2014; Mazloff et al., 2010), mixing is as highly temporally and spatially variable as its generating mechanisms (i.e., strong surface westerly winds and interaction of the currents and eddies with rough topography). Since the seminal work of Munk (1966)(Munk, 1966), bulk measures of mixing have found $K_v \sim \mathcal{O}(10^{-4})$ m^2 s^{-1} required to close the MOC(Ganachaud & Wunsch, 2000; Talley et al., 2003; Lumpkin & Speer, 2007; Talley, 2013) whereas estimates from profiling instruments often find $K_v \sim \mathcal{O}(10^{-5})$ m^2 s^{-1} in the ocean interior and much larger values only very close to the seafloor(Waterhouse et al., 2014). In the Diapycnal and Isopycnal Mixing Experiment in the Southern Ocean (DIMES), estimates of mixing based on microstructure profiles reported $K_v \sim \mathcal{O}(10^{-5})$ m^2 s^{-1} at the mean depth of an anthropogenic tracer released upstream of the Drake Passage but the tracer itself seemed to experience $K_v \sim \mathcal{O}(10^{-4})$ m^2 s^{-1} (Watson et al., 2013; Mashayek, Ferrari, et al., 2017). Figure 1 shows maps of diapycnal diffusivity in the SO constructed from local and non-local tidal mixing and mixing induced by waves generated due to interaction of Antarctic Circumpolar Currents and their overlying eddies with rough topography. While the maps are static (i.e. need to be interpreted as time-mean), they show significant horizontal and vertical variations over a range much larger than 10^{-5} $m^2 s^{-1}$ – 10^{-4} $m^2 s^{-1}$. One can imagine that changes to currents and eddies lead to significant temporal variability in these maps on timescales of days to months, whereas changes in underlying stratification can lead to changes in mixing patterns over centennial and longer timescales. In this work, we are concerned with the impact of variations in mixing on air-sea fluxes of CO_2.

The air-sea flux of CO_2 primarily depends on the difference in the partial pressures of CO_2 (pCO_2) between the atmosphere and the ocean. Oceanic pCO_2 is a function of dissolved inorganic carbon (DIC), temperature (T), salinity (S) and alkalinity (Alk). While the surface layer of the ocean is well mixed, there are strong gradients in the vertical distribution of these properties beneath the mixed layer. Physical processes such as mixing and biological processes like Net Community Production alter the physical and chemical properties of the surface waters, altering the pCO_2 of the surface (Mahadevan et al., 2011). The influence of altered diapycnal mixing on the surface pCO_2 is complex due to its coupled multivariate dependency (T,S,Alk,DIC) as well as the spatio-temporal variability in the biological and physical responses to variations in mixing (Dutreuil et al., 2009).

In this work, we evaluate the sensitivity of SO air-sea carbon fluxes to the variability of mixing within the SO by means of an eddy resolving ocean state estimate that includes a biogeochemical cycle and assimilates a host of in-situ and remote sensing data (Verdy & Mazloff, 2017). To explore the sensitivity of surface fluxes to mixing, we consider the two canonical values of diapycnal diffusivity, 10^{-4} m^2 s^{-1} and 10^{-5} m^2 s^{-1}, which is a conservative range given the much larger variations in mixing shown in Fig. 1. We show that the mixing in the upper ocean alters the distribution of DIC, alkalinity, temperature and salinity, resulting to changes in pCO_2 and air-sea CO_2 fluxes by 40% over a 6-year period.

Experiment Design

The biogeochemical Southern Ocean state estimate (B-SOSE) used here is a data-assimilating state estimate with an ocean resolution of 1/6° and 52 vertical layers, physics based on the MITgcm, and the NBLING biogeochemical model, as described fully in (Verdy & Mazloff, 2017). B-SOSE assimilates SOCATv5 and Argo data, including biogeochemical parameters from the SOCCOM float array, providing a baseline estimate of the ocean state that is dynamically consistent. For this study, we use the B-SOSE iteration-133 solution, which spans from Dec 2012 through Dec 2018. The full set of model parameters used in this 1/6° set up are given in (Swierczek et al., 2021). With regards to dif-

fusion, a vertical diffusivity is employed with values as discussed in the next paragraph, and a lateral biharmonic diffusivity is used with a value of 10^{-8} m^4s^{-1}. The GGL90 mixed layer parameterization of ggl90 is used, as is an implicit vertical diffusivity for convection of 10 m^2s^{-1}, and no mesoscale eddy parameterization was implemented (Gaspar, Grégoris, & Lefevre, 1990).

Two model simulations were carried out, each with a different constant background diffusivity value added to the surface generated model mixing. Ex1e-5 has a background diffusivity value of 10^{-5}, whilst Ex1e-4 has a background value of 10^{-4}, which prior to this work was the default value used in B-SOSE for optimization (Verdy & Mazloff, 2017). Comparing Ex1e-4 and Ex1e-5 provides a mechanistic understanding of how alterations to diapycnal mixing causes changes to carbon fluxes and to what extent over short timescales. Comparing experiments reflects how uncertainty in mixing parameterizations project on SO carbon fluxes. As mentioned in relation to Fig. 1, the range 10^{-5} m^2s^{-1}–10^{-4} m^2s^{-1} is conservative range, sandwiched between the two canonical paradigms of mixing often compared in Physical Oceanography.

Results

Carbon fluxes

Figure 2A shows the zonally integrated annual mean carbon fluxes for each of the six years of the model run. The SO is a net sink of atmospheric CO_2 (negative flux) at all latitudes each year with most of the uptake occurring between 45°S and 35°S, with a peak at 40°S, where around 7 Pg C $m^{-1}yr^{-1}$ is uptaken by the ocean. This strong uptake occurs since upwelling cold and nutrient rich deep circumpolar waters mix with mid-latitude warm waters, resulting in enhanced biological productivity and solubility driven uptake prior to subduction as Antarctic Intermediate Waters (Fig.2A,C). Higher latitudes show very low mean annual carbon fluxes, partly due to seasonal ice cover (Fig.2E,F). Near the polar front, just north of the maximum winter ice zone (Fig.2E-G pink and blue lines) a region of deep upwelling exists where CO_2 outgasses due to the upwelling of DIC rich old waters and inefficient biological uptake due to low temperatures and light limitation relative to the upward supply of DIC and nutrients.

The zonally integrated flux of carbon varies year on year, by almost 2 Pg C $m^{-1}yr^{-1}$ at some latitudes, with especially high inter annual variability seen at 60°S and 40°S (Fig.2A). These differences are likely to be due to varying oceanic conditions each year, some of which are associated with the Southern Annular Mode (SAM). A high SAM index is associated with stronger westerly winds over latitudes around 60°S, leading to stronger wind-induced upwelling and therefore enhanced outgassing.

The carbon fluxes also show strong seasonal trends (Fig.2C,E-G). In the summer (Dec to Feb), the northern SO latitudes are a source of carbon to the atmosphere, as high temperatures reduce the solubility of CO_2, with an exception being the waters around southern Australia (panels C,E). Although biological productivity will be high during summer due to higher temperatures and sunlight, the uptake of carbon by photosynthesis doesn't compensate for the reduced solubility due to temperature. In the south, lower temperatures allow the SO to act as a carbon sink even in the summer. Some outgassing still occurs at the upwelling zone of the polar front. Strong uptake of carbon can be seen in regions near topography, due to strong biological carbon draw down, and in the sub-polar gyres. Overall, between Jun-Aug, the SO is actually a net source of CO_2 to the atmosphere. In general, SO fronts, which mark sharp gradients in temperature and carbon chemistry, separate regions of net uptake from regions of outgassing.

In the winter (June - Aug), SO uptake of carbon is stronger than in summer due to colder temperatures and a deeper mixed layer, despite reduction in primary produc-

tivity (Fig.2C,F). Small regions of outgassing in the winter occur at the polar front and at the upwelling region on the west coast of South America, in the Argentine basin.

Increasing the background mixing from 10^{-5} m^2/s in Ex1e-5 to 10^{-4} m^2/s in Ex1e-4 leads to a significant change in the carbon flux which is noticeable even after one month (i.e. Dec 2012). The annual-mean zonally-integrated carbon uptake decreases at all latitudes for all years (Fig.2B). The greatest reduction in the uptake is at around 55°S, just north of the winter ice extent (Fig.2 B,H-J). Minor changes between the two experiments occur south of 65°S due to ice cover reducing carbon exchange in both experiments. The difference between experiments are also small north of 35°S.

The sensitivity of the flux is variable across the six years, showing inter-annual variability of up to 1.5 Pg C $m^{-1}yr^{-1}$ at 55°S (Fig.2B). This is within the range of the inter-annual variability of zonally integrated carbon fluxes themselves in Ex1e-5 (Fig.2A). A higher difference between experiments is seen for the first three years (2013 to 2015) than the final three years (2016 to 2018). The initially high differences between experiments are due to the abrupt change to mixing, altering the DIC-cline/alkalinity-cline/ halocline/thermocline of the upper ocean. As upper ocean mixing is never in an equilibrium state due to constantly changing winds, eddies and buoyancy fluxes, results from the first few months of this experiment do not seem unrealistically exaggerated due to the sudden perturbations to mixing in the real world. The maximum reduction in Ex1e-4 uptake, of 2.2 Pg C $m^{-1}yr^{-1}$, occurred at 52°S in 2014. By 2016, the DIC /alkalinity/salinity/temperature clines have settled down but the background fluxes across them remain different between Ex1e-5 and Ex1e-4. In the latter three years, the difference in carbon fluxes are up to a maximum of 1.5 Pg C $m^{-1}yr^{-1}$ at 45°S in 2016.

The difference in carbon fluxes between the two experiments also shows seasonal variability. Changes are the larger in the winter than the summer in almost all regions, with the exception of the very south where ice-coverage during the winter months reduces gas exchange in both experiments (Fig.2C).

In the winter, in almost all regions, Ex1e-4 has reduced carbon uptake as compared to Ex1e-5. The greatest decreases occur around 50°S, with strong reductions extending north into the Atlantic ocean. The Argentine basin is also a region of pronounced diminished carbon uptake (Fig.2I). Three small areas on the edge of the winter ice extent experience increased carbon uptake in the winter months (Fig.2I), the reason for this is discussed later in this paper.

In the summer, changes to carbon fluxes show more spatial variability than the winter months. At lower latitude outgassing regions, outgassing is decreased in Ex1e-4 (shown in blue), especially in the Argentine basin. A few exceptions to this include south of South Africa and in waters surrounding Tasmania (Fig.2H). Further south, where the SO is a sink for carbon, CO_2 uptake is reduced in Ex1e-4. The biggest reductions in uptake are seen in subpolar gyres and to the north of the winter ice extent, especially in the waters extending off the West Antarctic Peninsula.

The cumulative net flux of carbon into the ocean, integrated from 75°S northward to 30°S, is shown in (Fig.2D). In Ex1e-5, the total uptake is 1 Pg C yr^{-1}, whilst in Ex1e-4, only 0.6 Pg C yr^{-1} is taken up, a reduction of 0.4 Pg C yr^{-1}, equal to around 40%. The winter uptake is also reduced by 40% in Ex1e-4. These large percentage changes to carbon fluxes demonstrates the hypersensitivity of the system to diapycnal mixing. These numbers are for the six-year mean, and as panel B shows, the reductions are much higher over the first three years (almost double).

The cumulative fluxes are compared to other estimates of SO carbon flux integrated up to 45°S and 35°S for the period 2015-2017 (Fig.2D) (Bushinsky et al., 2019; Landschützer et al., 2016; Rödenbeck et al., 2013). At 45°S, the Ex1e-5 cumulative flux lies between the three observationally inferred estimates, while the Ex1e-4 estimate is slightly

lower. At 35°S, Ex1e-5 lies within the bounds of the three estimates, though appears to be towards the lower end, whilst Ex1e-4 is below. This suggests that the lower mixing Ex1e-5 may better represent the total carbon flux from atmosphere to the SO for the time frame studied.

0.1 Changes to surface ocean pCO_2

The partial pressure of CO_2 at the ocean surface (the pCO_2) controls air sea carbon fluxes, as carbon fluxes occur by diffusive processes due to the difference in pCO_2 between the atmosphere and the surface ocean. High (low) surface ocean pCO_2 vales result in regions of low (high) oceanic uptake, or even outgassing of CO_2 from the atmosphere (Fig.3A). A region of exception is under sea ice, where the diffusive flux of gases is prevented, meaning high pCO_2 differences between the atmosphere and the ocean don't correspond to carbon fluxes. The changes in carbon fluxes due to altered mixing, as seen in Figure2 are therefore due to changes in pCO_2. The pCO_2 of the surface ocean is set by salinity, temperature, DIC and alkalinity, meaning changes to pCO_2 are due to changes in the upper ocean concentration of any or all of these four tracers.

The annual mean pCO_2 of the surface ocean is higher in Ex1e-4 than Ex1e-5 in almost all regions, reducing the pCO_2 gradient between the atmosphere and the ocean, which results in a reduction in carbon uptake by the SO (Fig.3B). The areas of greatest increase in pCO_2 include South of South Africa and the waters east of the West Antarctic Peninsula. In a small number of areas, the annual mean pCO_2 is reduced in Ex1e-4, these areas include; at latitudes of around 30°S, especially to the east of Australia, the Argentine basin and a few small bands just off the Coast of Antarctica in the south, and these are regions where SO carbon uptake is increased in Ex1e-4 compared to Ex1e-5. Changes to pCO_2 also vary seasonally and correspond to the seasonality of changes to carbon fluxes, this will be discussed later in this paper.

Using the methodology set out by Takahashi *et al.* (2014) (Takahashi et al., 2014) we can calculate the pCO_2 changes due to changes in the upper 55m content of salinity, temperature, DIC and alkalinity individually.

$$\Delta pCO_2 = (\frac{\delta pCO_2}{\delta T})\Delta T + (\frac{\delta pCO_2}{\delta DIC})\Delta DIC + (\frac{\delta pCO_2}{\delta Alk})\Delta Alk + (\frac{\delta pCO_2}{\delta S})\Delta S \quad (1)$$

$$\frac{\delta pCO_2}{\delta T}\Delta T = 2(pCO_2)[Exp(0.0423(\pm 0.0002)\Delta T/2) - 1] \quad (2)$$

$$(\frac{\delta pCO_2}{\delta DIC}) = \gamma_{CO_2}(\bar{p}CO_2/\bar{T}CO_2) \quad (3)$$

$$\frac{\delta pCO_2}{\delta Alk} = \gamma_{ALK}(\frac{\bar{p}CO_2}{\bar{A}lk}) \quad (4)$$

$$(\frac{\delta pCO_2}{\delta S}) = 0.026(\pm 0.002) \cdot \bar{p}CO_2 \quad (5)$$

where $\bar{p}CO_2$ is the mean pCO_2 value, $\bar{A}lk$ is the mean alkalinity value, γ_{CO_2} is the Revelle factor for CO_2 (value used = 11), and γ_{ALK} is the Revelle factor for alkalinity (value used = -10).

The change in pCO_2 caused by changes to upper ocean tracer content is calculated, and is shown as a pCO_2 contribution for each of the four tracers (Fig.3D-G). The four individual contribution terms can then be summed together, resulting in the annual mean approximated change in pCO_2 (Fig.3C). The annual mean approximated change in pCO_2, obtained from summing the four contribution terms, is well matched to the changes to pCO_2 between the two experiments, verifying the assumptions made in Equations 2-5, and confirming that changes to the distribution of these tracers are key in causing changes to carbon fluxes (Fig.3B,C). The only region where the Takahashi *et al.* (Takahashi et

al., 2014) method does not seem to capture the changes is in the north of the SO, west of New Zealand and east of South America in the Argentine basin. This is likely due to enhanced water mass mixing occurring in these regions, making changes in this area complex to approximate with simple assumptions. This method also does not capture how strongly the carbon uptake is reduced in Ex1e-4 in the waters off the West Antarctic Peninsula.

On an annual basis, contributions from changes in upper ocean DIC and alkalinity content are the major drivers of changes in pCO_2, with the contributions from salinity and temperature changes being minimal (Fig.3E,F). An increase in alkalinity content decreases pCO_2, whilst an increase in salinity or DIC increases pCO_2. Where the temperature increases, pCO_2 increases due to the solubility effect. Increases in upper ocean DIC content in Ex1e-4 increases pCO_2 in the south, whilst in the north a decrease in DIC concentration decreases pCO_2. Conversely the increase in alkalinity concentration in the south decreases pCO_2, while the decrease in alkalinity in the north increases pCO_2. Changes in salinity concentrations act to slightly increase the pCO_2 in the south of Ex1e-4. Temperature changes cause a very slight decrease in pCO_2 in the north and an increase in the south. Overall the changes to pCO_2 from alkalinity dominate in the north and the pCO_2 is increased, whilst the changes in DIC, temperature and salinity dominate the changes to pCO_2 in the south, also increasing it (Fig.3I,J). This work demonstrates the importance of understanding how altering the diapycnal mixing is altering the upper ocean DIC and alkalinity content on short time scales, as this is what is causing changes to SO carbon fluxes.

Changes in DIC, alkalinity, temperature and salinity are all shown normalised by the standard deviation of each field. Due to the high standard deviation in the temperature field from 70°S to 30°S, changes relative to the standard deviation of temperature are multiplied by ten. The DIC, alkalinity and salinity content all increase in the south in Ex1e-4, with alkalinity increasing the most relative to its standard deviation. The upper ocean content of DIC, alkalinity and salinity all decrease in the northern SO (Fig.3I-K).The strongest contributions to changes in pCO_2 are not always due to the biggest changes in DIC /alkalinity /temperature or salinity. The changes to DIC and alkalinity content are both lower in the north than the south, but the resultant changes to pCO_2 are a similar magnitude, suggesting that the carbon chemistry is more sensitive to changes to DIC and alkalinity at the salinity and temperatures found in the north than in the south. The changes in salinity content are of a similar magnitude relative to its standard deviation as DIC and alkalinity, but has a minimal pCO_2 contribution, suggesting pCO_2 is not highly sensitive to salinity for the carbon system conditions (Fig.3G,K). Though changes to DIC are of a lower magnitude relative to its standard deviation when compared to alkalinity, the pCO_2 contributions from DIC are equal in magnitude to those from alkalinity, suggesting the system is highly sensitive to DIC concentration.

Vertical mixing across sharp tracer gradients

Figure 4 helps understand how changing diapycnal mixing, especially in the upper ocean, alters DIC, alkalinity and temperature distributions, thereby modifying the carbon fluxes. Strong correlations develop between locations with sharp vertical gradients of DIC and temperature and locations with significantly altered DIC content and temperatures with enhanced mixing (from Ex1e-5 to Ex1e-4) on timescales as short as half a month (Fig.4 A-D). The maximum change in DIC/ temperature is defined as the greatest difference in DIC/temperature concentration between the two experiments seen at any depth above 200 m at each latitude longitude in the domain. For DIC, regions experiencing high concentration changes with enhanced mixing are around the coast of Antarctica as well as in the Argentine basin. They clearly overlap with regions with the highest vertical gradients in concentration (Fig.4 A,B). Changes in alkalinity and salinity roughly follow a pattern similar to DIC (hence not shown). Changes in DIC, alka-

linity and salinity content in month one in regions where vertical gradients are low are minimal, as is the case for most of the SO. The greatest changes to temperature between experiments and the greatest vertical temperature gradients are also spatially well correlated (Fig.4 C,D). Strong changes occur in the northern SO, especially at around 90 east, in the Argentine basin, and in the waters surrounding New Zealand.

The changes to concentrations of alkalinity, DIC, salinity and temperature are key to changes in the oceanic pCO_2 as previously discussed. The largest change in their concentration between the two experiments occurs where there are sharp vertical tracer gradients, which are often in regions with low GGL90 parameterized mixing, as the strong vertical gradients generated by large-scale circulation and biological processes are not eroded by the model generated mixing. For DIC, salinity and alkalinity, these conditions are met around Antarctica where strong vertical gradients exist due to upwelling of abyssal waters. For temperature, the largest changes are in different regions from those of DIC and alkalinity. The mixing induced by surface winds at the air-sea interface can dwarf both the background values of Ex1e-5 and Ex1e-4, and allow the vertical gradients in tracers to become completely eroded, meaning that in stormy times and places the difference in tracer concentrations between the two experiments is minimal.

To further illustrate the correlation between the sharp vertical tracer gradients and changes in tracer concentration, (Fig.4E,F) we show the calculated correlation coefficient (R^2) value between the maximum vertical gradient at each latitude longitude and the maximum change in tracer concentration for various months. The highest R^2 values for all tracers occur in the first month of the perturbation (Dec 2012). Over time, although the magnitude of the change to tracers increases (Fig.4E), the correlation becomes weaker. By Dec 2018, the correlation has deteriorated as the lateral motions of eddies and currents have had a chance to have a leading order contribution to changes to tracer concentrations and their vertical gradients (MacGilchrist et al., 2019).

In the future with climate change, we can expect to see an increase in surface ocean temperature and increased vertical gradients in temperature (Li et al., 2020), increasing the sensitivity of surface temperature to diapycnal mixing. By contrast, Global Ocean Data Analysis Project (GLODAP) data predicts a decrease in the vertical gradient of DIC at relevant depths of 100 m to 300 m, making DIC driven changes to pCO_2 less sensitive to spatial variations in diapycnal mixing (Monteiro et al., 2010).

In Fig.4G we explore the seasonality of the correlation coefficients. After the first six months, a repeated seasonal cycle is established, with the highest R^2 value for DIC, salinity and alkalinity at the end of the summer. R^2 decreases through winter before increasing again rapidly during spring. The higher correlation during summers is likely due to sharper vertical tracer gradients, as the model GGL90 parameterization produces stronger mixing in the winter, eroding the vertical gradients. Thus, the change between Ex1e-5 and Ex1e-4 is less pronounced and therefore less correlated to vertical gradients in the winter. As for temperature, the initially a strong correlation declines over time albeit with a seasonal trend much different from that of DIC: highest correlation during the winter months, and lower during the summer. The seasonal cycle in R^2 for temperature is driven by strong R^2 values in the south. Conversely, the seasonal cycle seen for DIC is driven by seasonality and strong R^2 at lower latitudes. In other words, the seasonality in R^2 for each tracer comes from the regions with lower actual changes to tracer concentrations across the two experiments.

To further explore the action of our mixing perturbation on vertical gradients, (Fig.4) we look at the vertical structures of DIC and its gradient. In a zonal averaged sense looking at just the upper 130m of the water column in Ex1e-5, the highest DIC concentrations are in the deeper waters in the south, decreasing in concentration towards to surface and to the north (similar patterns hold for alkalinity). The surface waters towards the southern boundary of the SO are fed by wind-induced upwelling of deep waters which

are rich in DIC due to the respiration of organic material. As these waters are brought near the surface, they form strong vertical DIC concentrations. Further to the north, the upper 120m of the water column has weak vertical gradients of DIC concentration.

Filled contours in panel C shows the change in the vertical distribution of DIC due to the altered mixing over the first month, while the lines show its further temporal evolution. Waters south of 60°S and above depths of 40 m with the largest vertical DIC gradients experience the largest changes in concentration as discussed above. The dipole pattern implies the erosion of the sharp gradient by enhanced mixing. The DIC concentration increases with increased mixing in the upper surface waters (shown in red), whilst concentrations decrease between 40m and 20m depth (shown in blue). There is a clear divide at around 20m, above which the DIC concentration increases with increased mixing, whereas below this depth the concentration decreases. Panels D,E show latitudinal and longitudinal cross sections with the depth of the maximum vertical DIC gradient marked with black lines.

The diapycnal flux for a tracer is given by $-K_v \times \frac{\delta tracer}{\delta z}$ meaning the diapycnal flux of a tracer is proportional to the strength of the vertical tracer gradient, and to the prescribed diapycnal mixing value. Therefore if vertical diapycnal mixing K_v is increased, more DIC is mixed down gradient, meaning DIC is mixed upwards into the surface waters. This increase in upwards flux of DIC with an increase in K_v is the strongest where the DIC vertical gradient is the strongest, and results in the increase in DIC concentration in the surface waters. The increased upward flux of DIC with increased K_v below the depth of the maximum gradient is less than the increased upward flux at the depth of maximum gradient. Therefore, below depth of the maximum DIC vertical gradient, DIC concentrations are reduced due to a flux divergence, as more of this carbon has been mixed upwards into the surface waters. The depth of the maximum vertical DIC gradient is setting the depth above which DIC is increasing, and the magnitude of the maximum DIC vertical gradient sets the magnitude of differences in DIC concentration with altered mixing. Thus, as previously mentioned, a combination of high DIC gradients and enhanced background mixing leads to an increased upward flux of DIC, an enhanced surface concentration, and a reduced subsurface concentration in Ex1e-4 as opposed to Ex1e-5. Similar patterns hold for Alkalinity. Together, these changes lead to a significant change in oceanic surface pCO_2 and the carbon fluxes as described earlier.

We have assumed that all changes in DIC (and alkalinity) concentrations are due to changes in vertically fluxed DIC. In reality, some changes in DIC will be due to feedback from changes in surface temperature and nutrient concentrations effecting the associated biological productivity, which would alter DIC. Changes due to altered vertical fluxes of DIC have been shown to dominate over changes to DIC consumption by biology(Monteiro et al., 2010). Here too, the high correlation found between gradients and changes suggests that on these timescales DIC and alkalinity diapycnal mixing fluxes are the predominant drivers of the pCO_2 response in the SO.

Seasonal changes in pCO_2

The changes in carbon fluxes between experiments vary temporally as well as spatially, with much great differences in carbon fluxes in winter than in summer as was shown in Fig.2.

Following Eq. (1) and the discussion of Fig. 3, we can use the Takahashi *et al.* methodology(Takahashi et al., 2014) to also look at the seasonal changes to tracer contributions and their implications for the pCO_2. This is done in Fig6. Salinity contributions are not shown in the figure as they were negligible compared to contributions of DIC, alkalinity and temperature to changes in pCO_2. Changes to DIC and alkalinity, and their associated contributions to changes in pCO_2 are relatively constant regardless of season (Fig.6C-D,G-H). The vertical gradients of DIC and alkalinity are maintained all year as ocean circu-

lation continuously supplies DIC rich waters to the SO through upwelling. Slightly stronger changes to DIC and alkalinity concentrations in surface waters are expected in the summer months due to lower levels of wind-induced surface mixing, allowing for stronger vertical gradients to build up. This results in a higher sensitivity to changes to background diapycnal mixing. The depth of the maximum vertical gradient also deepens in the winter months as winter surface mixing deepens the DIC-cline (which shoals again in the spring).

Unlike the DIC and alkalinity contributions, the temperature contribution to changes in pCO_2 varies greatly between seasons (Fig.6B.F). In the summer, the change in temperature with increased mixing acts to reduce the surface ocean pCO_2, whilst in the winter it increases it. As with the work of (Precious Mongwe et al., 2018), we find that the overall changes to carbon fluxes depend on the interactive effects of changes to DIC, temperature and alkalinity, which can compensate or reinforce, and the predominant driver varies regionally and seasonally.

Changes to surface temperatures between Ex1e-4 and Ex1e-5 exhibit varying seasonal trends unlike changes to DIC and alkalinity, due to seasonal variations to the vertical structure of the thermocline (Fig.6I-N). During the summer, surface waters are warmer and temperature declines rapidly with depth down to 100 m. In the north SO, this trend continues more gradually to depths of 500 m. In the south, below 100 m the water temperature increases with depth due to the meridional overturning circulation and (more specifically the Ekman suction upwelling deep warmer waters of North-Atlantic origin; Fig.6I,J). In Ex1e-4, more subsurface cold waters are mixed towards the surface, resulting in cooler surface waters, and more warm waters from the surface are mixed down, warming sub surface temperatures relative to Ex1e-5 (Fig.6K). This results in regions with reduced outgassing in Ex1e-4 summer, mainly in the north (Fig.2H).

In July, during the austral winter, surface waters are well mixed and there is no temperature gradient in the upper 100 m (Fig.4J). Below the winter mixed layer in the south, the waters increase in temperature with depth due to the circulation of warmer waters from the North (Fig.4I,J). Enhanced mixing warms surface waters as more warm waters are upwelled from depth (Fig.4K), increasing the pCO_2. This signal, together with changes to DIC and alkalinity concentrations, result in a strong increase in winter pCO_2 and decreases carbon uptake in the south (Fig.2I). This increased surface temperature also results in reduced sea ice extent, especially towards the end of winter/ spring, due to faster sea ice melt in Ex1e-4. This reduced sea ice is responsible for the very small regions of increased carbon uptake seen in the southern winter in Ex1e-4, despite the increased pCO_2 in winter (Fig.2 I, J).

During southern winter at lower latitudes further north, the temperature decreases with depth, similar to what is seen in the summer, and increased mixing results in cooler surface waters. At around 50°S, the general trend of change in the surface water temperatures is less clear. This could be due to warmer surface waters in the south travelling north as part of the upper branch of global circulation, and the effect of the decreased surface water temperatures in the north. These two effects oppose each other and reduce the net change in surface water temperatures.

Because the change in surface temperature and associated change to pCO_2 vary in sign with season (mostly positive/negative in winter/summer), the annual mean change in temperature and its contribution to changes in pCO_2 deceptively average out annually (Fig.3D), but are nevertheless key to driving the seasonal response of changing SO carbon fluxes in response to altered diapycnal mixing.

The changes to the mixed layer depth between the two experiments is also highly seasonal. In the summer months, the mixed layer depth is unchanged between the two experiments, with a mean difference of ¡ 1 m across the whole SO in January. However,

in the winter months, the mixed layer is deepened in Ex1e-4 by an average of 21 m in the July. This increase contributes to the increased winter pCO_2 of surface waters observed in Ex1e-4, as a deeper mixed layer allows for an increased entertainment of deep waters, thereby increasing the flux of warmer DIC rich waters to the surface. This explains why the DIC contribution to the increase in pCO_2 is slightly greater in July than in January (Fig.6 C,G) despite higher vertical gradients in DIC (and therefore stronger sensitivity) expected during summer.

1 Discussion

Figure 7 compares the pCO_2 values for Ex1e-4 and Ex1e-5 to 2013-2018 observed levels from the Surface Ocean CO_2 Atlas (SOCAT(Bakker et al., 2016)). Panel A shows the magnitude of difference between Ex1e-4 and SOCAT observations relative to the magnitude of difference between Ex1e-5 and SOCAT. Regions shown in red represent an area where Ex1e-5 pCO_2 is closer to observations than the pCO_2 of Ex1e-4. Neither of the two experiments is clearly matching to SOCAT observations better than the other. Regional trends are also unclear, though from the limited data available, Ex1e-5 appears to better represent the pCO_2 of the northern Pacific Ocean, as well as off the coast of South Africa and Tasmania. Meanwhile estimates from Ex1e-4 are better matched to observations in the western Atlantic and the northern Indian Oceans.

Panel B shows the probability density function for the difference between SOCAT and B-SOSE for the two experiments, broken down over seasons. In the summer, Ex1e-4 and Ex1e-5 both have a similar spread, with the mean difference of 15.5 atm for Ex1e-5, lower than 17.46 atm for Ex1e-4 (same trend holds for the modal values). The high-end tails of the distributions are more skewed than the the lower ends, implying a systematic over-estimate by B-SOSE. In other words, the model over estimates the flux of carbon from ocean to atmosphere, or underestimates the SO carbon uptake from the atmosphere, particularly in the summer.

SOCAT data is heavily biased towards summer data due to limitations on data collection in the winter. The mean difference between SOCAT and B-SOSE is lower for the winter-mean than for the summer in both experiments. Averaging the field plotted in panel A suggests that overall Ex1e-5 does a better job in comparison with SOCAT but not by much. Two major issues stand between achieving better agreement between ocean models (such as ours) and observations (such as SOCAT), one observational and one computational.

First, mixing is highly spatiotemporally variable. To achieve a close agreement with observations, a model should have a representation of such variability. Global and SO models don't resolve many of the processes responsible for diapycnal mixing and so resort to parameterizations(Gaspar, Grégoris, & Lefevre, 1990; Large et al., 1994). In the Southern Ocean, such parameterization primarily induce strong turbulence under the seasonal atmospheric storm tracks, mixing the DIC gradients in the upper few hundreds of meters. In other places, such as under the ice or when there is not a strong wind-induced turbulence, the models rely on a prescribed background value for turbulent diffusivity. It is the background value that is behind the hypersensitivity of fluxes discussed in this work. Turbulence can exist under the sea-ice due to bottom generated lee waves penetrating all the way to the top boundary where they can induce large vertical velocities (Baker & Mashayek, in press) or due to shoaling of remotely generated internal tides (de Lavergne et al., 2020), among other processes not accounted for in climate models. Furthermore, there are nuances to physics of small scale turbulent mixing that which are not considered in climate models, but can easily extend the range of variations to the background mixing beyond what was considered herein (Mashayek, Salehipour, et al., 2017; Cimoli et al., 2019). Even a crude time-mean estimate for the combined tidal and lee-wave-induced mixing shows significant mixing under the seasonal sea-ice (e.g. Fig. 1).

Second, despite the significant investments in observations such as SOCAT, Fig. 7A clearly shows the sparsity of the available data. From a statistical perspective, this coverage is insufficient to discern which background mixing value better represents the real ocean despite the strong impact of these choices on pCO_2. This issue can be resolved only through sustained observations. The strong seasonal cycle in the changes to carbon fluxes indicates the importance of year round observations, and knowledge of the seasonal cycle of pCO_2 is worse in the SO than in most other regions of the ocean (Bushinsky et al., 2019).

2 Conclusion

In summary, we showed that the air-sea carbon fluxes in the Southern Ocean are hypersensitive to modest background mixing variations that are well within the range of our best estimates of the uncertainty associated with mixing rates in the Southern Ocean. Given the seasonal (and even shorter) timescales on which mixing can vary over orders of magnitude in time and space in the upper SO, this result highlights the absolute necessity for climate models to resolve the spatiotemporal variability of small scale turbulent mixing or skillfully parameterize them.

Part of the reason behind the lack of appreciation of this result to date is the widespread mindset that the relevance of diapycnal mixing for carbon fluxes manifests itself through changes to the regional and global overturning circulation. While that may be true on centennial timescales, here we show that on much faster timescales mixing directly acts upon tracers such as DIC, alkalinity, temperature, and salinity in such a way that almost instantly changes the surface ocean pCO_2 sufficiently to lead to a significant change in surface ocean fluxes. Thus, this work encourages a distinction between the timescales on which small scale sub-grid scale turbulent mixing in the SO can act on the tracers explicitly through eroding their gradients and implicitly through changing the background ocean circulation.

Acknowledgments

Modeling: MM

Analyses: EE

Writing - original draft: EE

Writing - review and editing: AM, MM

3 Data and material availability

The data sets generated during and/or analysed during the current study are available from the corresponding author on reasonable request

References

Adkins, J. F. (2013, 9). The role of deep ocean circulation in setting glacial climates. *Paleoceanography*, *28*(3), 539–561. Retrieved from `http://doi.wiley.com/10.1002/palo.20046` doi: 10.1002/palo.20046

Alford, M. H. (2003). Redistribution of energy available for ocean mixing by long-range propagation of internal waves. *Nature*, *423*(6936), 159–162.

Baker, L., & Mashayek, A. (in press). Surface reflection of bottom generated oceanic lee waves. *Journal of Fluid Mechanics*.

Bakker, D. C., Pfeil, B., Landa, C. S., Metzl, N., O'Brien, K. M., Olsen, A., ... Xu, S. (2016, sep). *A multi-decade record of high-quality fCO2 data in version 3 of the Surface Ocean CO2 Atlas (SOCAT)* (Vol. 8) (No. 2). Retrieved from `https://essd.copernicus.org/articles/8/383/2016/` doi:

10.5194/essd-8-383-2016

Bushinsky, S. M., Landschützer, P., Rödenbeck, C., Gray, A. R., Baker, D., Mazloff, M. R., ... Sarmiento, J. L. (2019, 11). Reassessing Southern Ocean Air-Sea CO2 Flux Estimates With the Addition of Biogeochemical Float Observations. *Global Biogeochemical Cycles*, *33*(11), 1370–1388. Retrieved from https://onlinelibrary.wiley.com/doi/abs/10.1029/2019GB006176 doi: 10.1029/2019GB006176

Cessi, P. (2019). The global overturning circulation. *Annual review of marine science*, *11*, 249–270.

Cimoli, L., Caulfield, C. P., Johnson, H. L., Marshall, D. P., Mashayek, A., Naveira Garabato, A. C., & Vic, C. (2019, 12). Sensitivity of Deep Ocean Mixing to Local Internal Tide Breaking and Mixing Efficiency. *Geophysical Research Letters*, *46*(24), 14622–14633. Retrieved from https://onlinelibrary.wiley.com/doi/abs/10.1029/2019GL085056 doi: 10.1029/2019GL085056

Cimoli, L., et al. (2021). Significance of diapycnal mixing within the Atlantic Meridional Overturning Circulation. *Nature Communications*, *Under review*.

de Lavergne, C., Vic, C., Madec, G., Roquet, F., Waterhouse, A. F., Whalen, C. B., ... Hibiya, T. (2020, 5). A Parameterization of Local and Remote Tidal Mixing. *Journal of Advances in Modeling Earth Systems*, *12*(5), e2020MS002065. Retrieved from https://onlinelibrary.wiley.com/doi/abs/10.1029/2020MS002065 doi: 10.1029/2020MS002065

Devries, T. (2014, 7). The oceanic anthropogenic CO2 sink: Storage, air-sea fluxes, and transports over the industrial era. *Global Biogeochemical Cycles*, *28*(7), 631–647. Retrieved from http://doi.wiley.com/10.1002/2013GB004739 doi: 10.1002/2013GB004739

DeVries, T., & Primeau, F. (2011, 12). Dynamically and Observationally Constrained Estimates of Water-Mass Distributions and Ages in the Global Ocean. *Journal of Physical Oceanography*, *41*(12), 2381–2401. Retrieved from https://journals.ametsoc.org/jpo/article/41/12/2381/11258/Dynamically-and-Observationally-Constrained doi: 10.1175/JPO-D-10-05011.1

Doney, S. C., Lindsay, K., Caldeira, K., Campin, J. M., Drange, H., Dutay, J. C., ... Yool, A. (2004). Evaluating global ocean carbon models: The importance of realistic physics. *Global Biogeochemical Cycles*. doi: 10.1029/2003GB002150

Dutreuil, S., Bopp, L., & Tagliabue, A. (2009). Impact of enhanced vertical mixing on marine biogeochemistry: Lessons for geo-engineering and natural variability. *Biogeosciences*, *6*(5), 901–912. Retrieved from www.biogeosciences.net/6/901/2009/ doi: 10.5194/bg-6-901-2009

Ganachaud, A., & Wunsch, C. (2000). Improved estimates of global ocean circulation, heat transport and mixing from hydrographic data. *Nature*, *408*(6811), 453–457.

Garabato, A. C. N., Frajka-Williams, E. E., Spingys, C. P., Legg, S., Polzin, K. L., Forryan, A., ... others (2019). Rapid mixing and exchange of deep-ocean waters in an abyssal boundary current. *Proceedings of the National Academy of Sciences*, *116*(27), 13233–13238.

Garabato, A. C. N., Polzin, K. L., King, B. A., Heywood, K. J., & Visbeck, M. (2004). Widespread intense turbulent mixing in the southern ocean. *Science*, *303*(5655), 210–213.

Garabato, A. C. N., Stevens, D. P., Watson, A. J., & Roether, W. (2007). Short-circuiting of the overturning circulation in the Antarctic Circumpolar Current. *Nature*, *447*(7141), 194–197.

Gaspar, P., Grégoris, Y., & Lefevre, J.-M. (1990). A simple eddy kinetic energy model for simulations of the oceanic vertical mixing: Tests at station papa and long-term upper ocean study site. *Journal of Geophysical Research: Oceans*,

95(C9), 16179–16193.

Gaspar, P., Grégoris, Y., & Lefevre, J.-M. (1990, sep). A simple eddy kinetic energy model for simulations of the oceanic vertical mixing: Tests at station Papa and long-term upper ocean study site. *Journal of Geophysical Research*, *95*(C9), 16179. Retrieved from http://doi.wiley.com/10.1029/JC095iC09p16179 doi: 10.1029/JC095iC09p16179

Gnanadesikan, A., Dunne, J. P., Key, R. M., Matsumoto, K., Sarmiento, J. L., Slater, R. D., & Swathi, P. S. (2004). Oceanic ventilation and biogeochemical cycling: Understanding the physical mechanisms that produce realistic distributions of tracers and productivity. *Global Biogeochemical Cycles*, *18*(4), 1–17. Retrieved from https://agupubs.onlinelibrary.wiley.com/doi/pdf/10.1029/2003GB002097https://pdfs.semanticscholar.org/09bf/eb7e7728fb8ad30f253e13e72adf20992330.pdf doi: 10.1029/2003GB002097

Gruber, N., Landschützer, P., & Lovenduski, N. S. (2019). The variable southern ocean carbon sink. *Annual review of marine science*, *11*, 159–186.

Intergovernmental Panel on Climate Change. (2014). *Climate Change 2014: Synthesis Report. Contribution of Working Groups I, II and III to the Fifth Assessment Report of the Intergovernmental Panel on Climate Change*. Intergovernmental Panel on Climate Change.

Klocker, A. (2018). Opening the window to the Southern Ocean: The role of jet dynamics. *Science Advances*. doi: 10.1126/sciadv.aao4719

Landschützer, P., Gruber, N., & Bakker, D. C. E. (2016, 10). Decadal variations and trends of the global ocean carbon sink. *Global Biogeochemical Cycles*, *30*(10), 1396–1417. Retrieved from http://doi.wiley.com/10.1002/2015GB005359 doi: 10.1002/2015GB005359

Large, W. G., McWilliams, J. C., & Doney, S. C. (1994). Oceanic vertical mixing: A review and a model with a nonlocal boundary layer parameterization. *Reviews of geophysics*, *32*(4), 363–403.

Ledwell, J. R., St. Laurent, L. C., Girton, J. B., & Toole, J. M. (2011). Diapycnal mixing in the antarctic circumpolar current. *Journal of Physical Oceanography*, *41*(1), 241–246. Retrieved from http://www.rocklandscientific.com doi: 10.1175/2010JPO4557.1

Li, G., Cheng, L., Zhu, J., Trenberth, K. E., Mann, M. E., & Abraham, J. P. (2020, 12). Increasing ocean stratification over the past half-century. *Nature Climate Change*, *10*(12), 1116–1123. Retrieved from http://www.nature.com/articles/s41558-020-00918-2 doi: 10.1038/s41558-020-00918-2

Lumpkin, R., & Speer, K. (2007). Global ocean meridional overturning. *Journal of Physical Oceanography*, *37*(10), 2550–2562.

MacGilchrist, G. A., Garabato, A. C. N., Brown, P. J., Jullion, L., Bacon, S., Bakker, D. C., ... Torres-Valdés, S. (2019). Reframing the carbon cycle of the subpolar southern ocean. *Science advances*, *5*(8), eaav6410.

Mahadevan, A., Tagliabue, A., Bopp, L., Lenton, A., Mémery, L., & Lévy, M. (2011, 5). Impact of episodic vertical fluxes on sea surface pCO2. *Philosophical Transactions of the Royal Society A: Mathematical, Physical and Engineering Sciences*, *369*(1943), 2009–2025. Retrieved from https://royalsocietypublishing.org/doi/10.1098/rsta.2010.0340 doi: 10.1098/rsta.2010.0340

Marinov, I., & Gnanadesikan, A. (2011, 2). Changes in ocean circulation and carbon storage are decoupled from air-sea CO₂ fluxes. *Biogeosciences*, *8*(2), 505–513. Retrieved from https://bg.copernicus.org/articles/8/505/2011/ doi: 10.5194/bg-8-505-2011

Marinov, I., Gnanadesikan, A., Sarmiento, J. L., Toggweiler, J. R., Follows, M., & Mignone, B. K. (2008). Impact of oceanic circulation on biological carbon storage in the ocean and atmospheric pCO2. *Global Biogeochemical Cycles*.

doi: 10.1029/2007GB002958

Marshall, J., & Speer, K. (2012). Closure of the meridional overturning circulation through Southern Ocean upwelling. *Nature Geoscience*, *5*(3), 171–180. Retrieved from www.nature.com/naturegeoscience doi: 10.1038/ngeo1391

Mashayek, A., Ferrari, R., Merrifield, S., Ledwell, J., St Laurent, L., & Garabato, A. (2017). Topographic enhancement of vertical turbulent mixing in the Southern Ocean. *Nature Communications*, *8*. doi: 10.1038/ncomms14197

Mashayek, A., Salehipour, H., Bouffard, D., Caulfield, C. P., Ferrari, R., Nikurashin, M., ... Smyth, W. D. (2017). Efficiency of turbulent mixing in the abyssal ocean circulation. *Geophysical Research Letters*, *44*(12), 6296–6306.

Mazloff, M. R., Heimbach, P., & Wunsch, C. (2010). An eddy-permitting Southern Ocean state estimate. *Journal of Physical Oceanography*, *40*(5), 880–899. Retrieved from https://journals.ametsoc.org/view/journals/phoc/40/5/2009jpo4236.1.xml doi: 10.1175/2009JPO4236.1

Melet, A., Hallberg, R., Legg, S., Nikurashin, M., Melet, A., Hallberg, R., ... Nikurashin, M. (2014, 3). Sensitivity of the Ocean State to Lee Wave–Driven Mixing. *Journal of Physical Oceanography*, *44*(3), 900–921. Retrieved from http://journals.ametsoc.org/doi/abs/10.1175/JPO-D-13-072.1 doi: 10.1175/JPO-D-13-072.1

Monteiro, P. M., Monteiro, P. M., Monteiro, P. M., Monteiro, P. M., Monteiro, P. M., Monteiro, P. M., ... Monteiro, P. M. (2010, 12). A Global Sea Surface Carbon Observing System: Assessment of Changing Sea Surface CO2 and Air-Sea CO2 Fluxes. In *Proceedings of oceanobs'09: Sustained ocean observations and information for society* (pp. 702–714). European Space Agency. Retrieved from http://www.oceanobs09.net/proceedings/cwp/cwp64 doi: 10.5270/oceanobs09.cwp.64

Munk, W. H. (1966). Abyssal recipes. In *Deep sea research and oceanographic abstracts* (Vol. 13, pp. 707–730).

Nikurashin, M., & Ferrari, R. (2010, 5). Radiation and Dissipation of Internal Waves Generated by Geostrophic Motions Impinging on Small-Scale Topography: Theory. *Journal of Physical Oceanography*, *40*(5), 1055–1074. Retrieved from http://journals.ametsoc.org/doi/abs/10.1175/2009JPO4199.1 doi: 10.1175/2009JPO4199.1

Nikurashin, M., & Vallis, G. (2011). A theory of deep stratification and overturning circulation in the ocean. *Journal of Physical Oceanography*, *41*(3), 485–502.

Orsi, A. H., Whitworth, T., & Nowlin, W. D. (1995, may). On the meridional extent and fronts of the Antarctic Circumpolar Current. *Deep Sea Research Part I: Oceanographic Research Papers*, *42*(5), 641–673. Retrieved from https://www.sciencedirect.com/science/article/pii/096706379500021W doi: 10.1016/0967-0637(95)00021-W

Precious Mongwe, N., Vichi, M., & Monteiro, P. M. (2018, 5). The seasonal cycle of pCO2 and CO2 fluxes in the Southern Ocean: Diagnosing anomalies in CMIP5 Earth system models. *Biogeosciences*, *15*(9), 2851–2872. Retrieved from https://bg.copernicus.org/articles/15/2851/2018/ doi: 10.5194/bg-15-2851-2018

Rödenbeck, C., Keeling, R. F., Bakker, D. C. E., Metzl, N., Olsen, A., Sabine, C., & Heimann, M. (2013, 3). Global surface-ocean <i>p</i>^{CO₂} and sea–air CO₂ flux variability from an observation-driven ocean mixed-layer scheme. *Ocean Science*, *9*(2), 193–216. Retrieved from https://os.copernicus.org/articles/9/193/2013/ doi: 10.5194/os-9-193-2013

Sarmiento, J. L., Gruber, N., Brzezinski, M. A., & Dunne, J. P. (2004). High-latitude controls of thermocline nutrients and low latitude biological productivity. *Nature*. doi: 10.1038/nature02127

Schmittner, A., Urban, N. M., Keller, K., & Matthews, D. (2009). Using tracer observations to reduce the uncertainty of ocean diapycnal mixing and climate-carbon cycle projections. *Global Biogeochemical Cycles*, *23*(4). Retrieved from http://www.nodc. doi: 10.1029/2008GB003421

Shakespeare, C. J. (2020). Interdependence of internal tide and lee wave generation at abyssal hills: Global calculations. *Journal of Physical Oceanography*, *50*(3), 655–677.

Sigman, D. M., Hain, M. P., & Haug, G. H. (2010). *The polar ocean and glacial cycles in atmospheric CO2 concentration* (Vol. 466) (No. 7302). doi: 10.1038/nature09149

Swierczek, S., Mazloff, M. R., Morzfeld, M., & Russell, J. L. (2021, jul). The effect of resolution on vertical heat and carbon transports in a regional ocean circulation model of the argentine basin. *Journal of Geophysical Research: Oceans*, *126*(7), e2021JC017235. Retrieved from https://onlinelibrary.wiley.com/doi/10.1029/2021JC017235 doi: 10.1029/2021jc017235

Takahashi, T., Sutherland, S. C., Chipman, D. W., Goddard, J. G., & Ho, C. (2014). Climatological distributions of pH, pCO2, total CO2, alkalinity, and CaCO3 saturation in the global surface ocean, and temporal changes at selected locations. *Marine Chemistry*. doi: 10.1016/j.marchem.2014.06.004

Talley, L. D. (2013). Closure of the global overturning circulation through the Indian, Pacific, and southern oceans. *Oceanography*, *26*(1), 80–97. Retrieved from http://dx.doi.org/10.5670/oceanog.2013.07 doi: 10.5670/oceanog.2013.07

Talley, L. D., Feely, R. A., Sloyan, B. M., Wanninkhof, R., Baringer, M. O., Bullister, J. L., ... Zhang, J. Z. (2016, 1). Changes in Ocean Heat, Carbon Content, and Ventilation: A Review of the First Decade of GO-SHIP Global Repeat Hydrography. *Annual Review of Marine Science*, *8*, 185–215. Retrieved from www.go-ship.org doi: 10.1146/annurev-marine-052915-100829

Talley, L. D., Reid, J. L., & Robbins, P. E. (2003). Data-based meridional overturning streamfunctions for the global ocean. *Journal of Climate*, *16*(19), 3213–3226.

Tamsitt, V., Abernathey, R. P., Mazloff, M. R., Wang, J., & Talley, L. D. (2018). Transformation of Deep Water Masses Along Lagrangian Upwelling Pathways in the Southern Ocean. *Journal of Geophysical Research: Oceans*. doi: 10.1002/2017JC013409

Verdy, A., & Mazloff, M. R. (2017). A data assimilating model for estimating Southern Ocean biogeochemistry. *Journal of Geophysical Research: Oceans*, *122*(9), 6968–6988. Retrieved from http://hycom.org doi: 10.1002/2016JC012650

Waterhouse, A. F., Mackinnon, J. A., Nash, J. D., Alford, M. H., Kunze, E., Simmons, H. L., ... Lee, C. M. (2014). Global patterns of diapycnal mixing from measurements of the turbulent dissipation rate. *Journal of Physical Oceanography*. doi: 10.1175/JPO-D-13-0104.1

Watson, A. J., Ledwell, J. R., Messias, M. J., King, B. A., Mackay, N., Meredith, M. P., ... Garabato, A. C. N. (2013). Rapid cross-density ocean mixing at mid-depths in the Drake Passage measured by tracer release. *Nature*, *501*(7467), 408–411.

Watson, A. J., & Naveira Garabato, A. C. (2006). The role of Southern Ocean mixing and upwelling in glacial-interglacial atmospheric CO2 change. *Tellus, Series B: Chemical and Physical Meteorology*, *58*(1), 73–87. Retrieved from https://www.tandfonline.com/action/journalInformation?journalCode=zelb20 doi: 10.1111/j.1600-0889.2005.00167.x

4 Figures

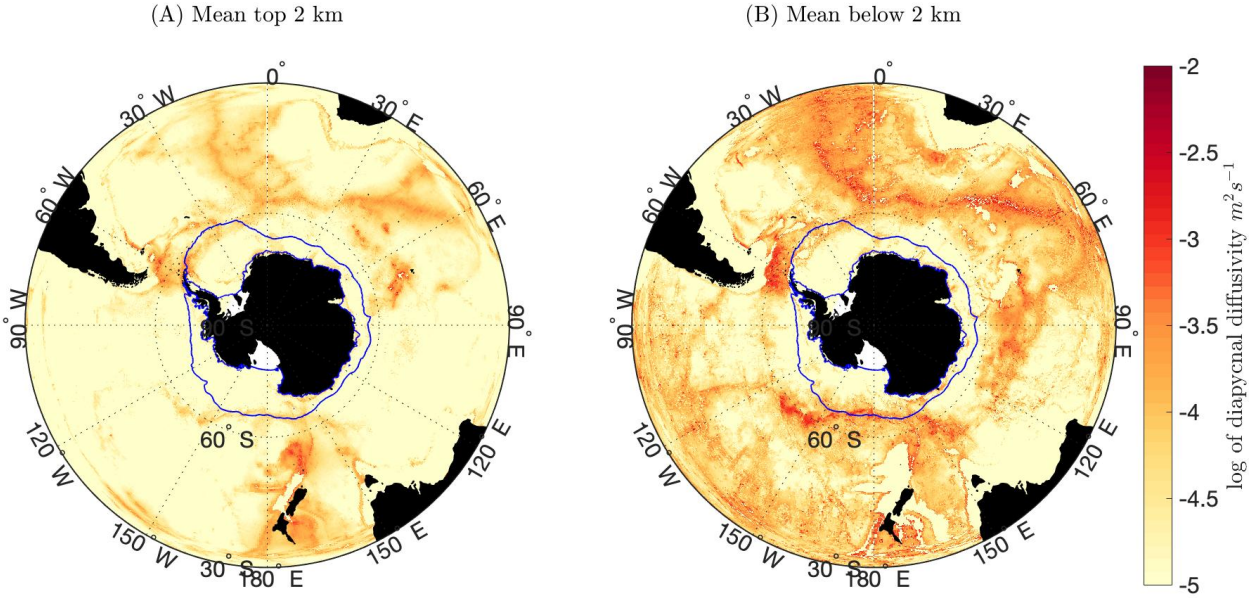

Figure 1: Distribution of turbulent diapycnal mixing in the Southern Ocean, constructed from local and non-local tidal mixing estimates of deLavergne *et al.* (2020) (de Lavergne et al., 2020) and estimates of mixing due to interaction of geostrophic currents and eddies with rough topography from Nikurashin and Ferrari (2013). Annual mean sea ice extent shown in blue

778

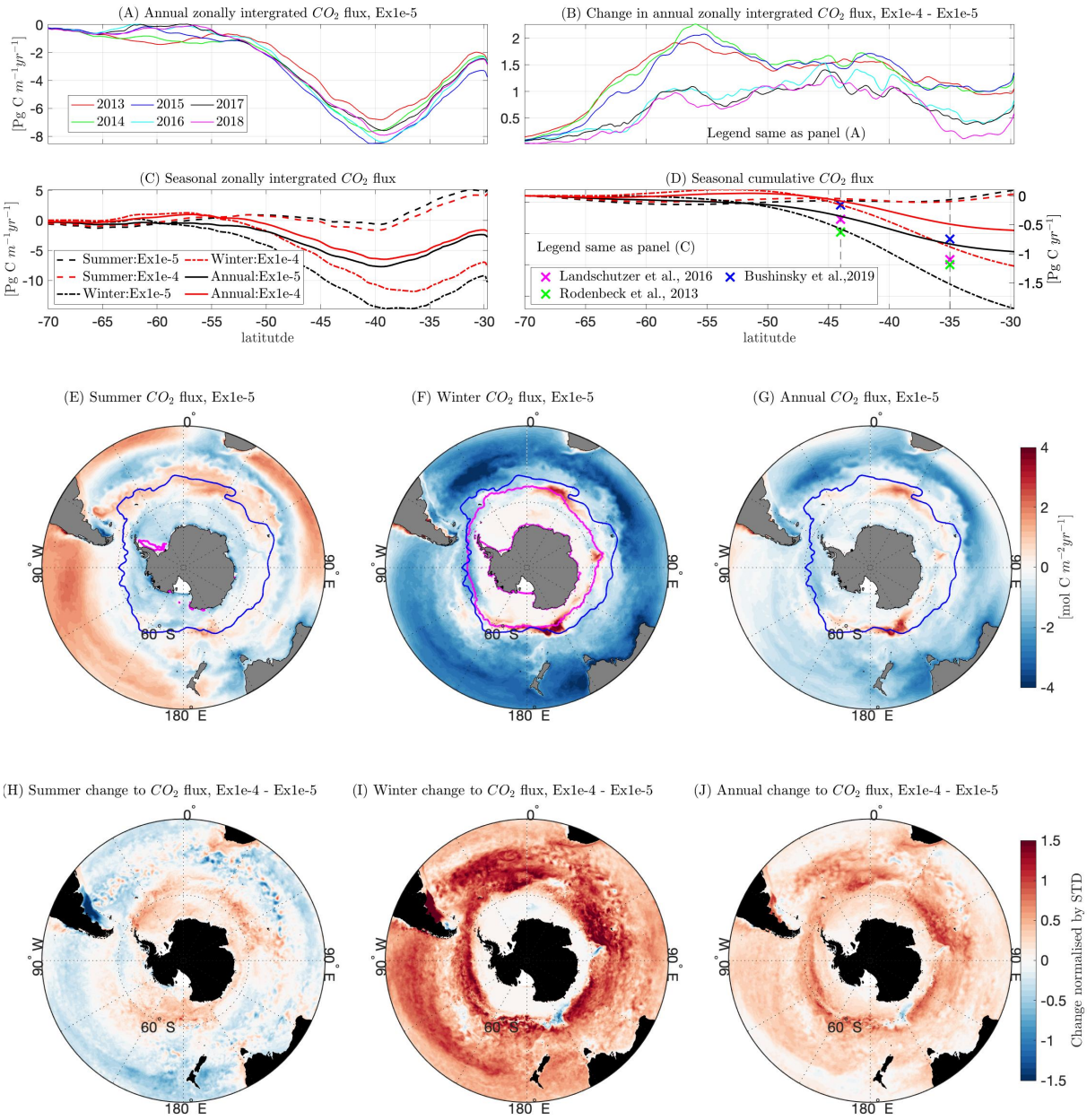

Figure 2: Air - Sea CO_2 fluxes show significant changes with altered diapycnal mixing rates. (A) Zonally integrated flux of CO_2 for each year of Ex1e-5 (negative = Carbon flux from atmosphere to ocean). (B) Difference between between Ex1e-4 and Ex1e-5 in the zonal integrated flux of CO_2 for each year of the experiment. (C) Zonal integrated flux for summer (dashed, Dec to Feb), Winter (dotted, June -Aug) and Annual (solid) for Ex1e-4 (red) and Ex1e-5 (Black). (D) Cumulative sum of carbon fluxes from 70°S northward to 30°S (legend same as previous panel). Observational markers are included for comparison (Landschützer et al., 2016; Bushinsky et al., 2019; Rödenbeck et al., 2013). (E-G) Average summer, winter and annual carbon fluxes for Ex1e-5. Summer and winter sea-ice extents are shown by magenta lines in panels E and F. Blue shows the Polar Front as defined by (Orsi et al., 1995) (H-J) Average difference (Ex1e-4 –Ex1e-5) in CO_2 flux for summer, Winter and Annual, normalized by the standard deviation of the Ex1e-5 annual mean (positive = reduced carbon uptake or increased outgassing).

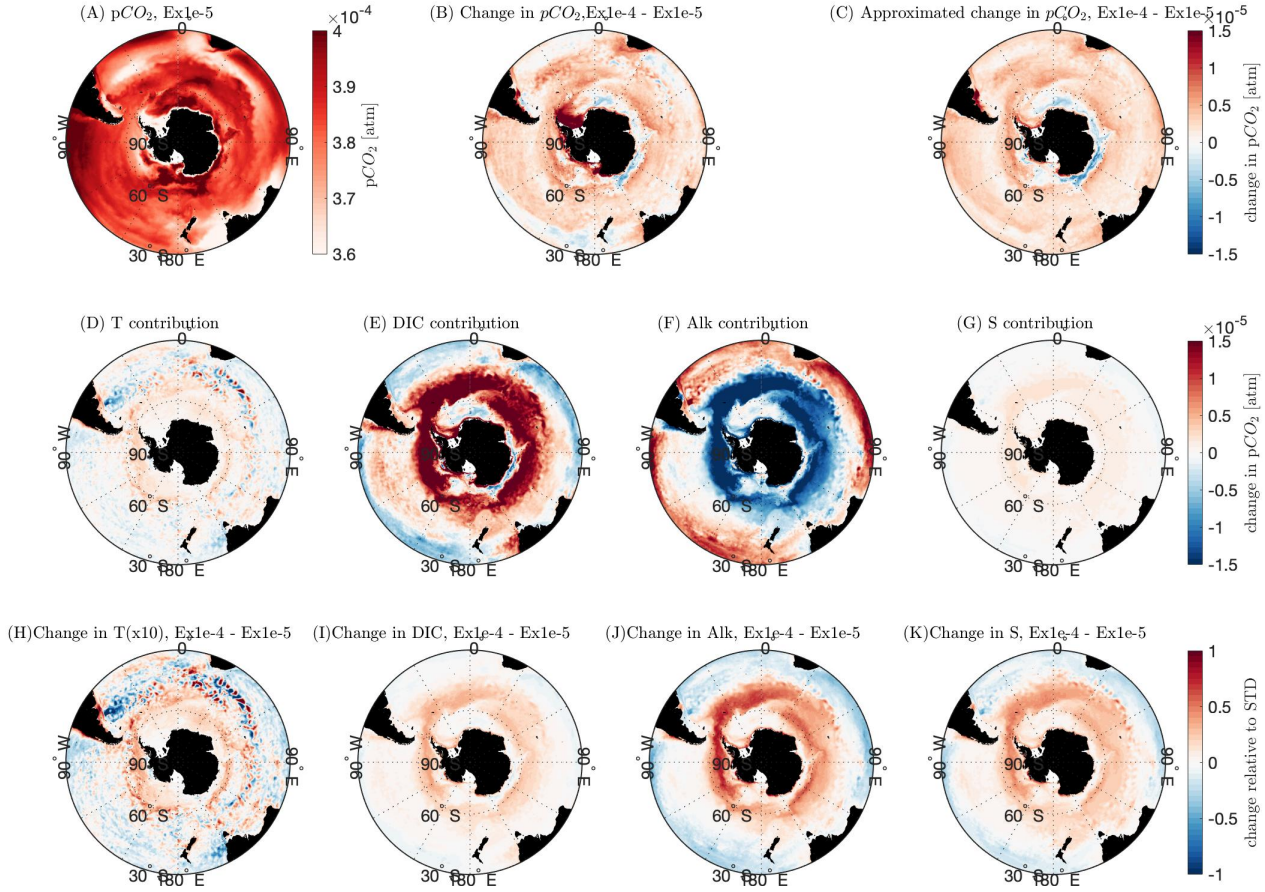

Figure 3: Changes to surface (upper 55m) DIC and alkalinity concentrations are responsible for changes to surface ocean partial pressure and carbon fluxes.(A) Annual mean surface ocean pCO_2 in Ex1e-5.(B) Change in pCO_2 between Ex1e-4 and Ex1e-5. (C) Same as panel B, but this time changes to pCO_2 approximated based on the methodology of Takahashi et al. (2014) (Takahashi et al., 2014) that breaks down the change into various contributions as per equations (1-5). The various contributions are shown in panels (D-G). (H-K) Annual mean change in potential temperature, DIC, alkalinity and Salinity, normalized by standard deviation of each field all for Ex1e-5.

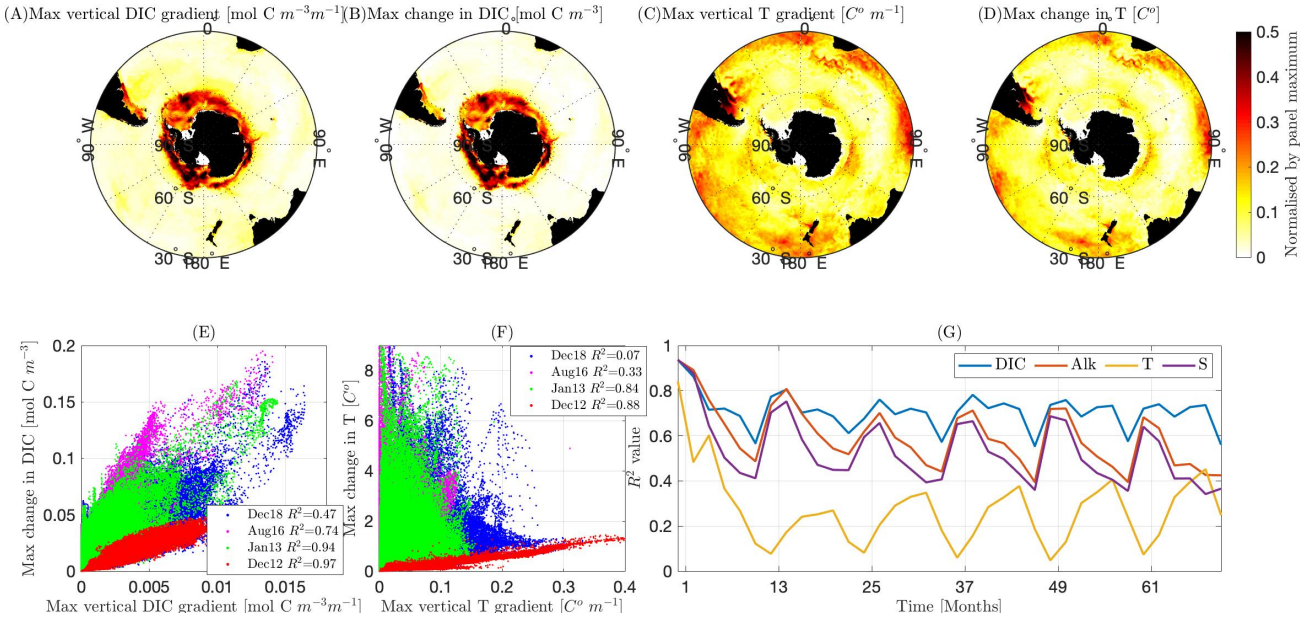

Figure 4: Maximum change in tracer concentrations due to the perturbation to diapycnal mixing is corresponds to regions with high vertical gradients of tracer concentration. (A) Maximum vertical DIC gradient in the water column for Ex1e-5 midway through the first month(??-check with Matt) of the simulation (Dec 2012), normalised by maximum contour value. (B) Maximum change to DIC between the two experiments (i.e. Ex1e-4 - Ex1e-5), normalised by the maximum contour value. (C,D) Same as A and B but for temperature. (E,F) Scatter plots showing the correlation between maximum vertical gradient and maximum change to tracer concentration for each lat-lon, with the corresponding R^2 values shown in the legend; Panel E is for DIC and panel F for temperature. (G) Correlation R^2 as a function of time for DIC, alkalinity, temperature and salinity

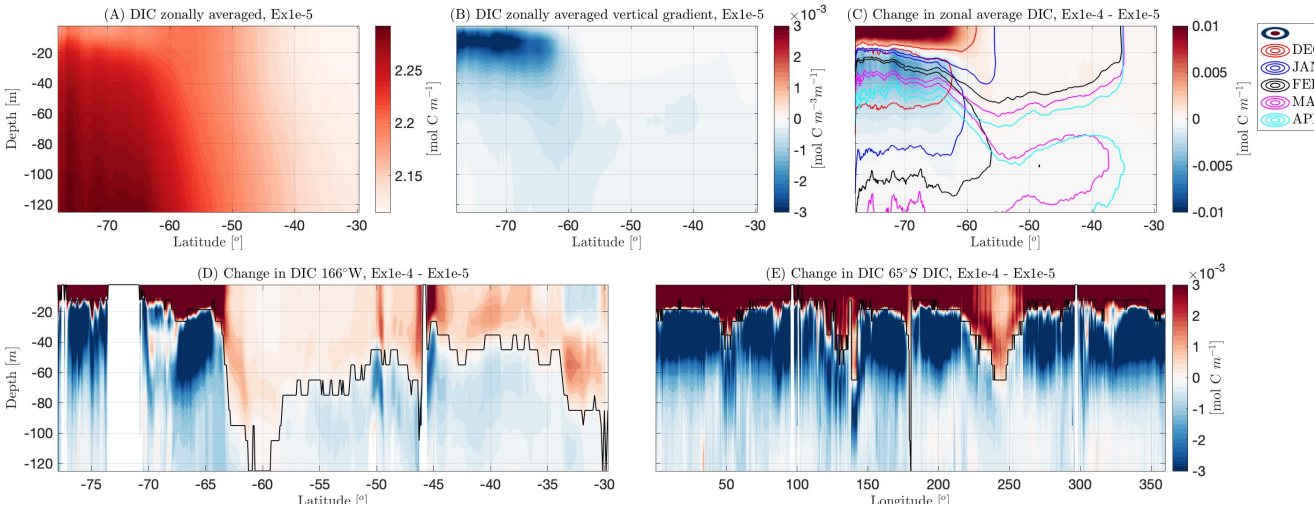

Figure 5: All for the first month of the simulations (Dec 2012): (A) zonal average DIC concentration in Ex1e-5. (B) zonal average DIC vertical gradient in Ex1e-5–blue indicates decrease in concentration towards the surface. (C) zonal average change in DIC concentration (Ex1e-4 - Ex1e-5)–filled contours shows Ex1e-4 - Ex1e-5 with blue/red indicating decreased/increased DIC concentration. Contour lines highlight the $+/-2e^{-3}$ mol C m^{-3} contour levels, illustrating the expansion of the signal over time. Similar patterns exist for alkalinity and salinity (not shown). (D) Latitudinal cross section of change in DIC at 166°W. Depth of maximum vertical DIC gradient for Ex1e-5 is marked by a black line. (E) Longitudinal cross section of change in DIC at 65°S.

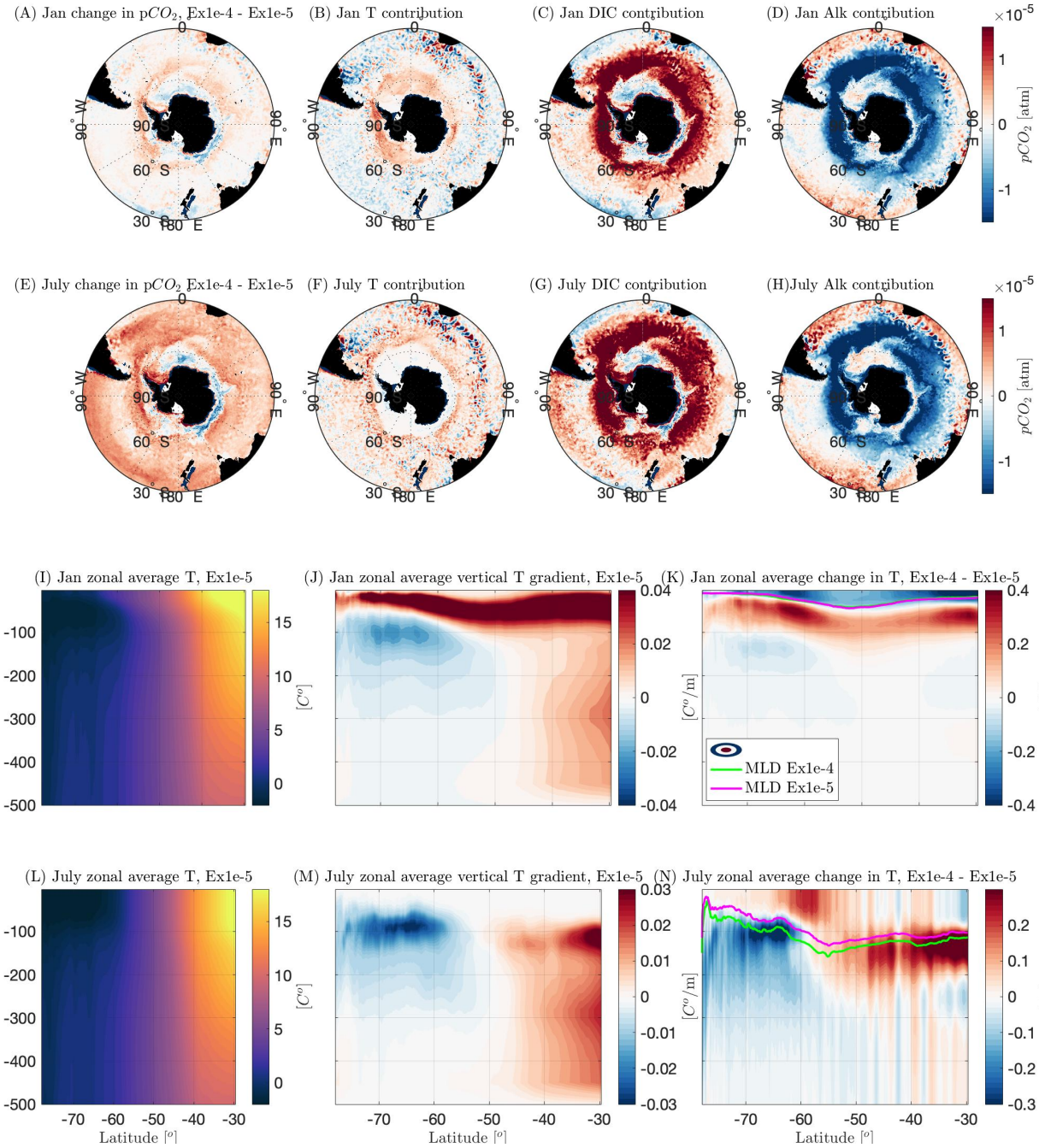

Figure 6: (A)January (summer; 2013-2018 mean) change in pCO_2 (i.e. Ex1e-4 - Ex1e-5) approximated by the method of (Takahashi et al., 2014) and its breakdown (as per Eqs. 1) to contributions due to changes in temperature (B), DIC (C), and alkalinity (D).(E-H) Same as A-D but for July (Winter; 2013-2018 mean). (I-K) January (2013-2018 mean) zonally averaged distributions in the upper 500m for Temperature (I), temperature vertical gradient (J; red implies increase in temperature towards the surface), and change in temperature between the two experiments with the mixed layer depth (MLD) for Ex1e-5 (pink) and Ex1e-4(green) overlain. (L- N) Same as I-J but for July.

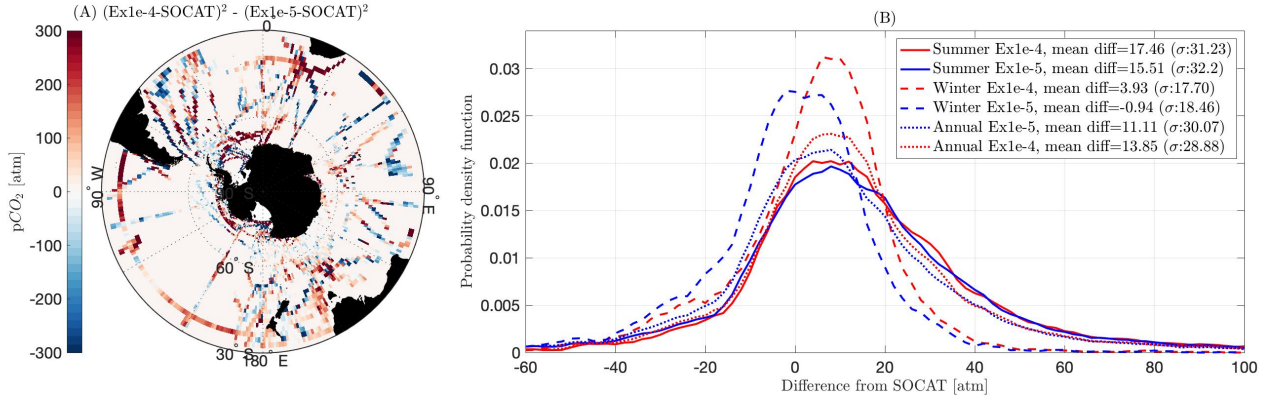

Figure 7: Comparison of modelled carbon fluxes to observations from Surface Ocean CO_2 Atlas (SOCAT) between 2012 and 2018 (Bakker et al., 2016). (A) Comparison of the differences between the two experiments and SOCAT: red/blue shows regions where Ex1e-5/Ex1e-4 is closer to the observations. (B) Probability density function showing the misfit between observed carbon fluxes from SOCAT and the model output for pCO_2.